Chemosphere 344 (2023) 140344

Contents lists available at ScienceDirect

Chemosphere

journal homepage: www.elsevier.com/locate/chemosphere

Comparison of the photocatalytic degradability of PFOA, PFOS and GenX using Fe-zeolite in water

Junying Wen [a], Huarui Li [a,b], Lars Ditlev Mørck Ottosen [a], Johan Lundqvist [c], Leendert Vergeynst [a,*]

[a] Centre for Water Technology (WATEC) & Department of Biological and Chemical Engineering, Aarhus University, Universitetsbyen 36, 8000, Aarhus C, Denmark
[b] School of Civil Engineering, Yantai University, 30, Qingquan RD, Laishan District, Yantai, 264005, PR China
[c] Department of Biomedical Sciences and Veterinary Public Health, Swedish University of Agricultural Sciences, Box 7028, SE-750 07, Uppsala, Sweden

HIGHLIGHTS

- Photocatalytic degradation of GenX was lower than for PFOA and PFOS after 7 h.
- Overall defluorination of GenX (33%) is lower than for PFOA (69%) and PFOS (51%).
- GenX (40%) adsorbed less than PFOA (99%) and PFOS (87%) on Fe-zeolite.
- Short-chain (<C4) transformation products were resistant to degradation.
- GenX produced higher levels of persistent ultra-short-chain transformation products.

GRAPHICAL ABSTRACT

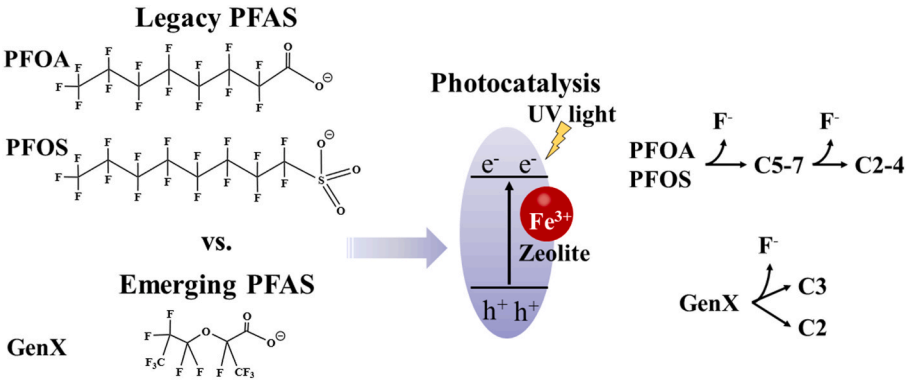

ARTICLE INFO

Handling editor: Sergi Garcia-Segura

Keywords:
Poly- and perfluorinated alkyl substances
Photocatalysis
Hexafluoropropylene oxide dimer acid
Fe-zeolite
Defluorination
Degradation pathway

ABSTRACT

Knowledge on the photocatalytic degradability of the emerging poly- and perfluorinated alkyl substances (PFAS) in water, specifically GenX, is limited. GenX has been detected globally in river water and is considered potentially more toxic than legacy PFAS. In this study, we compared the photocatalytic degradability of GenX with the legacy compounds perfluorooctanoic acid (PFOA) and perfluorooctanesulfonic acid (PFOS) using Fe-zeolite photocatalysts. After 7 h of irradiation, GenX showed lower removal (79%) and defluorination (33%) as compared to PFOA (100% removal and 69% defluorination) and PFOS (100% removal and 51% defluorination). The quasi-first-order degradation rate of GenX (1.5 h^1) was 12 and 1.2 times lower than PFOA (18.4 h^{-1}) and PFOS (1.8 h^{-1}), respectively. Additionally, PFOA's defluorination rate (0.9 h^{-1}) was approximately 2.6 and 9 times higher than GenX (0.35 h^{-1}) and PFOS (0.1 h^{-1}), respectively. These outcomes correlate with GenX's lower hydrophobicity, leading to reduced adsorption (40%) compared to PFOA (99%) and PFOS (87%). Based on identified transformation products, we proposed a GenX degradation pathway, resulting in ultra-short-chain PFASs with a chain length of 2 and 3 carbon atoms, while PFOA and PFOS degraded stepwise, losing 1 carbon-fluorine bond at a time, leading to gradually shorter chain lengths (from 7 to 2 carbon atoms). In conclusion, GenX is more challenging to remove and degrade due to its lower adsorption on the photocatalyst,

* Corresponding author.
E-mail address: leendert.vergeynst@bce.au.dk (L. Vergeynst).

https://doi.org/10.1016/j.chemosphere.2023.140344
Received 8 August 2023; Received in revised form 26 September 2023; Accepted 30 September 2023
Available online 4 October 2023

potential steric hindrance, and higher production of persistent ultra-short-chain transformation products through photocatalysis.

1. Introduction

Poly- and perfluoroalkyl substances (PFAS) are a group of anthropogenic chemicals that has been recognized as high-risk water pollutants (Olvera-Vargas et al., 2022). In the last two decades, PFAS have been used in a wide range of applications (Crone et al., 2019; Glüge et al., 2020) and have been detected in drinking water sources worldwide (Thompson et al., 2011; Rahman et al., 2014; Glüge et al., 2020; Liu et al., 2021a). Their perfluorinated moieties with strong C–F bonds and polar heads provide PFAS an amphipathic character and low reactivity (Vakili et al., 2021) resulting in high environmental persistence, tendency for bio-accumulation and half-life times in humans of several years (Li et al., 2018a). The ubiquitous presence of PFAS poses therefore a risk to humans (Li et al., 2018b; Vakili et al., 2021). For these reasons, two of the most produced and used PFAS, perfluorooctanoate acid (PFOA) and perfluorooctane sulfonate (PFOS), are banned in the European Union and the United States of America (Pierozan and Karlsson, 2021).

Since the ban of legacy PFAS, alternative fluorinated shorter-chain congeners are introduced as substitutes (Vakili et al., 2021). For example, hexafluoropropylene oxide dimer acid (GenX) was introduced in 2009 as the substitute for PFOA, which was believed to entail lower risk for human health due to its lower tendency for bio-accumulation (Vakili et al., 2021). However, more than a decade of releasing GenX into the environment has led to its detection in natural waters worldwide (Hopkins et al., 2018). Concentration of up to 4 μg/L were detected in drinking water wells and lakes nearby industrial plants in North Carolina, USA (Hopkins et al., 2018). It has also been detected in rivers in Europe at concentration of 11–73 ng/L (Gebbink et al., 2017; Vakili et al., 2021). Furthermore, recent reports based on *in vitro* assays showed that GenX is more likely to induce apoptosis in the human liver cells than PFOA (Yoo et al., 2021) and has higher potency than PFOA and PFOS as agonist for the human peroxisome proliferator-activated receptor alpha (Evans et al., 2022). In response to such alarming effects, the European Chemicals Agency has added GenX to the candidate list of substances of very high concern for authorization in 2019 (ECHA, 2019). In 2022, the US Environmental Protection Agency (EPA, 2022) issued a limit for GenX of 10 pg/L in drinking water.

Destructive methods such as photocatalysis to degrade PFAS in water have been drawing increasing attention (Liu et al., 2022; Li et al., 2023). Even though photocatalysis has shown great potential for degrading PFAS in water, studies have mainly focused on the legacy PFAS such as PFOA and PFOS (Qian et al., 2020, 2021; Xu et al., 2020; Wen et al., 2022; Xia et al., 2022), and only one study was found investigating the emerging GenX (Zhu et al., 2022). Zhu et al. (2022) reported that an adsorptive photocatalyst synthesized by depositing bismuth onto the activated-carbon supported titanate nanotubes (1 g/L), was able to adsorb GenX (100 μg/L, pH 7.0) within 1 h followed by 70% degradation and 43% mineralization of the adsorbed GenX under 254 nm UV light in 4 h.

In this study, the overall goal was to compare the efficacy of Fe-doped zeolite photocatalyst to degrade GenX, PFOA and PFOS. The specific objectives were to (1) compare the degradation and defluorination of GenX, PFOA and PFOS, (2) identify the transformation products and (3) elucidate the degradation pathway of GenX on Fe-zeolite.

2. Materials and methods

2.1. Chemicals and materials

Individual standard stock solutions of 10 mM of trifluoroacetic acid (TFAA), perfluoropropanoic acid (PFPrA), perfluoroheptanoic acid (PFHpA), perfluoropentanoic acid (PFPeA), heptafluorobutyric acid (PFBA), nanofluoro-1-butanesulfonic acid (PFBS), undecafluorohexanoic acid (PFHxA), pentadecafluorooctanoic acid (PFOA), heptadecafluorooctanesulfonic acid (PFOS) and perfluoro(2-methyl-3-oxahexanoic) acid (GenX) were prepared in methanol and stored at 4 °C. 30 mM NaOH was added to the stock solutions of the perfluoroalkyl carboxylic acids to prevent esterification (EPA, 2019). Suppliers of all chemicals are specified in Table S1. Plastic volumetric flasks and bottles for preparing and storing PFAS solutions were made of high-density polyethylene (HDPE) or polypropylene (PP) and purchased from VWR.

2.2. Synthesis of the photocatalyst

The Fe-doped zeolite was synthesized from zeolite β, hydrogen (surface area of 620 m^2/g, SiO_2:Al_2O_3 of 360:1, average particle size of 1 μM) using a wet-impregnation method followed by calcination (Jamalluddin and Abdullah, 2014). Zeolite (0.5 g) was mixed with 45 mL of deionized water and shaken for 1 h. Then, 5 mL of a 1 M $FeSO_4$ water solution was added, and the mixture was shaken for 24 h. The solid was washed 3 times with deionized water and recovered by centrifugation. Afterward, the solid was dried at 60 °C overnight and calcined for 4 h at 500 °C under air with a temperature ramp of 2 °C/min.

2.3. Analytical methods

2.3.1. Ultra-high pressure liquid chromatography - mass spectrometry

Ultra-high performance liquid chromatography (UHPLC, UltiMate 3000 UHPLC, Thermo Fischer Scientific) coupled to a time of flight mass spectrometer (Q-TOF-MS, Bruker Compact) with electrospray ionization source was used to identify and quantify PFASs (Table S2 presents the detailed parameters of MS). Standard solution for external calibration (0.001, 0.003, 0.006, 0.01, 0.03, 0.06, 0.1, 0.3, 0.5 μmol/L) were prepared by dilution of the methanol stock solution (10 mM) in 50/50 water/methanol.

Chromatographic separation was carried out using an Acquity UPLC HSS T3 column (2.1 mm × 100 mm, 1.8 μm particle size; Waters, The United States). After comparing different methods, an LC method from Janda et al. (2019) showed the best separation and detection of the targeted PFAS (detailed information listed in Table S3). For the final LC method, a binary gradient (eluent A: 2 mM ammonium formate and 0.2% formic acid in deionized H_2O/methanol (4:1, v/v), eluent B: 2 mM ammonium formate in methanol) was applied at a flow rate of 250 μL/min at 35 °C and an injection volume of 5 μL. The gradient was as follows: 2 min pre-injection equilibration time at 12.5% B, following a rise to 75% in 3 min, and further rise to 97.5% in 6 min; next, 97.5% eluent B was held for 4 min. Finally, the eluent was switched back to 12.5% B for 5 min.

The instrumental precision was expressed as the relative standard deviation of the peak areas. Instrumental detection limits were estimated following the Eurachem Guide (Vergeynst et al., 2017).

$$IDL = b + 2 \times t_{1-\beta,n-1} \times SD$$

Where b is the mean blank level, n is the number of replicates (n = 3). The Student t-value with β (0.05) and n (3) is 2.92, and SD is the standard deviation of the peak area at the lowest concentration level where a non-noise peak could be integrated. Blank and calibration standard solutions were analyzed in triplicate.

The instrumental linearity was investigated by comparing the lack of fit of a linear and quadratic function, determined by $1/x^2$ weighted least squares regression. As a combined measure of imprecision and model fit, the root mean square of the relative errors (RMSE) of the calibration curves was calculated as follows (Vergeynst et al., 2017):

$$RMSE = \sqrt{\frac{\sum_i^n \left(\frac{y_i - \widehat{y_i}}{\widehat{y_i}}\right)^2}{n-p}}$$

where y_i is the i^{th} measured peak area and $\widehat{y_i}$ is the predicted peak area of the regression function with p parameters through n data point.

2.3.2. Ion chromatography

Ion chromatography (IC) (Thermo Scientific) equipped with a Dionex IonPac AS23 (2 × 250 mm) analytical column with a guard column (Dionex Ionpac AG23, 2 × 50 mm) and Thermo Scientific DS6 heated conductivity detector was used for measuring fluoride ions (F^-) following previous work (Arana Juve et al., 2022). The eluent was 45 μM sodium carbonate and 8 μM sodium bicarbonate at a rate of 0.25 mL/min.

Defluorination is defined as the ratio of the concentration of F^- in water to the total fluorine in the parent PFAS molecule:

$$Defluorination\ (\%) = \frac{C_{F^-}}{C_0 \times the\ number\ fluorine\ atoms\ of\ the\ PFAS}$$

where C_{F^-} and C_0 are the concentrations of F^- ions and initial concentration of PFAS (μM). The number of fluorine atoms in PFOA, PFOS and GenX are 15, 17 and 11, respectively.

2.4. Photocatalytic degradation of PFAS

The initial concentration of the individual working solutions of PFOA, PFOS and Gen X was 10 μM in deionized water, which were prepared from a 2 mM stock solution on the day of conducting the experiments. Individual PFAS solutions (150 mL) were degraded with Fe-zeolite photocatalyst (1 g/L) in triplicate in quartz reactors of 12 cm diameter and 1.8 cm height with quartz lids exposed to UV light (Sankyo Denki G8T5, UV-C) with a wavelength of 254 nm (5 mW/cm^2) for 0 min, 30 min, 1 h, 2 h, 4 h and 7 h without stirring.

3. Results

3.1. Validation of analytical method

We documented the method precision, instrumental detection limits (IDLs), and linearity for the parent compounds GenX, PFOA, and PFOS, and degradation products PFHxA, PFBA, PFBS, PFPrA, and TFAA. The method precision, expressed as the relative standard deviation of peak areas, was generally below 15% for all compounds, except for PFPrA (16%) at 0.003 μM concentration. IDLs ranged from 0.0001 to 0.007 μM, except for TFAA, which had an IDL of 0.043 μM (Table S4). Linear regression yielded RMSE values ranging from 9% to 19%, except for PFOS (25%) and PFBS (28%) (Table S4). Quadratic regression produced RMSE values ranging from 9% to 13%, except for PFBS (31%) and TFAA (34%), indicating non-linear responses over the entire range (Table S4). Throughout the study, linear ranges of the multi-point external calibration curves were used to determine concentrations.

3.2. PFAS removal

In comparison to the undoped zeolite, Fe-doping the zeolite substantially increased the photocatalytic defluorination from 6 ± 3% to 29 ± 3% for GenX after 1 h, from 8 ± 0% to 59 ± 3% for PFOA after 1 h, and from 12± 2% to 51± 2% for PFOS after 7 h (Fig. S1). These results demonstrate the effectiveness of the Fe-doping method and the role of Fe in enhancing the photocatalysis.

After 7 h irradiation in the presence of Fe-zeolite, GenX showed the lowest removal from the water phase (79 ± 18%) whereas PFOA and PFOS were undetectable (Fig. 1a). In the first 30 min, PFOA was completed removed from the water phase while during the same time 73% 2 ± of PFOS and 40% 0 ± of GenX were removed. After 2 h, GenX reached a plateau with 20% remaining in the water phase, while PFOS was gradually removed between 0.5 and 4 h.

The following quasi-first-order model has been proposed to estimate the apparent photocatalytic removal rate of PFAS on the heterogeneous photocatalysts (Liu et al., 2014), under the assumption that adsorption-desorption rates are substantially faster than degradation rates:

$$ln\left(\frac{C_0}{C}\right) = k_{app}t \quad (1)$$

where C_0 and C are the water-phase concentrations of the PFAS initially and during the reaction as a function of time (t, h), and k_{app} (h $^{-1}$) the apparent rate constant.

Calculated by Equation (1), the apparent rate constant of PFOS was estimated to be 1.8 h^{-1} within the first hour, which was 1.2 times higher than the apparent rate constant of 1.5 h^{-1} of GenX within the first 2 h (Fig. 1b). While PFOA was undetectable after 30 min in the water, we estimated its apparent rate constant to be 18.4 h^{-1} by considering its detection limit (0.001 μM).

Equation (2) describes the linearized relationship between the fluoride concentration in the aqueous phase (C_{F^-}) and the initial concentration of total fluorine in the parent compound ($C_{TF,0}$; 150, 170 and 110 μM for PFOA, PFOS and GenX, respectively) as a function of time (t, h) and the rate constant (k, h^{-1}) (Ašperger, 2003)

$$ln\left(1 - \frac{C_{F^-}}{C_{TF,0}}\right) = -kt \quad (2)$$

Based on the data from Fig. 3, the defluorination (Fig. 1c) for PFOA (0.9 h^{-1}) was approximately 2.6 and 9 times higher than that of GenX (0.35 h^{-1}) and PFOS (0.1 h^{-1}), respectively.

3.3. Transformation products

Overall, we detected perfluoroalkyl carboxylic acids (PFCAs) as degradation products for each parent compound. Additionally, fluoride and formic acid ($HCOO^-$) were detected by IC as degradation products for all compounds at all analyzed time points. The pH was monitored at various time intervals (Table S5), showing a progressive decline in the water phase, likely due to the generation of formic acid. PFOA (Fig. 2b) and PFOS (Fig. 2c) degraded by losing one carbon-fluorine bond at a time, resulting in a gradually shortening chain length from 7 to 2 carbon atoms. Consequently, PFCAs with chain lengths of 5–7 carbon atoms first appeared and then disappeared, while PFCAs with less than 4 carbon atoms and fluoride accumulated as the reactions progressed. PFHpA (C7) and PFHxA (C6) concentrations were generally the lowest, reaching maxima of 0.007–0.27 μM after 0.5–1 h, and then decreased below the detection limit. PFPeA (C5) reached slightly higher concentrations of 0.58–3 μM after 0.5–4 h and subsequently decreased. The ultra-short-chain degradation products PFBA (C4), PFPrA (C3), and TFAA (C2) gradually increased to 2–6 μM, 1.7–2 μM, and 0.85–0.95 μM, respectively, during the 7 h of the reaction. Fluoride, as the terminal degradation product, reached concentrations of 104 μM and 87 μM after 7 h for PFOA and PFOS, respectively.

In contrast, during the photocatalytic reaction of GenX, only 2 ultra-short-chain PFAS with 3 (PFPrA) and 2 (TFAA) carbon atoms as well as fluoride have been detected in the water phase (Fig. 2a). The concentrations of PFPrA, TFAA and fluoride increased during the first 2 h and then remained relatively constant at about 8, 4 and 37 μM, respectively.

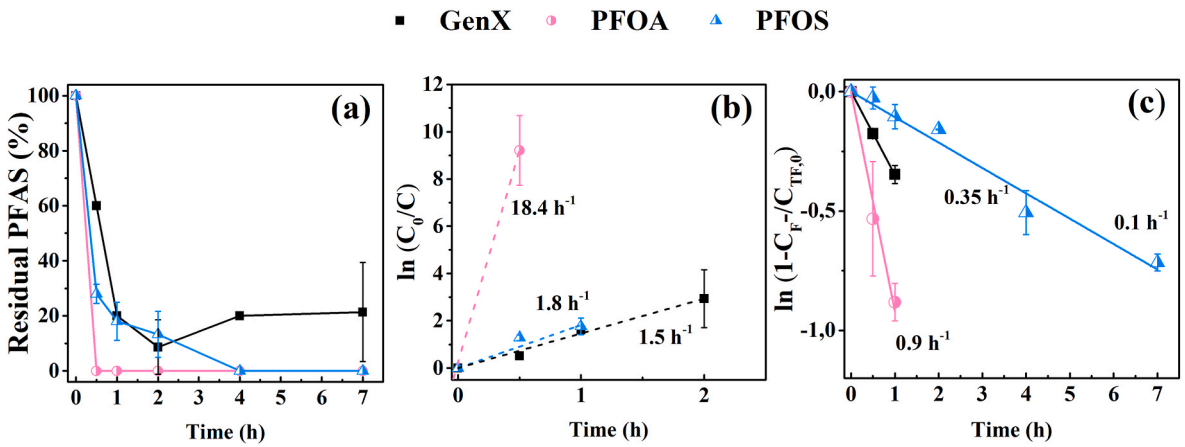

Fig. 1. Removal (a), first order removal rates (b) and first order defluorination rates (c) of GenX, PFOA and PFOS. The initial concentration for each parent compound was 10 μM with 1 g/L Fe-zeolite in the reaction mixture (n = 3). The pH decreased gradually during the experiment from 4.44 to 4.98 to 3.88–4.58 (Table S4).

3.4. Fluorine balance

For each PFAS, fluorine mole balances were calculated by summing the number of organic-bound fluorine atoms in the measured PFAS and the inorganic fluoride in the water phase. The distribution of organic and inorganic fluorine in the water phase was obtained from this calculation (Fig. 3). Overnight adsorption (4 °C) on Fe-zeolite (1 g/L) resulted in 99 ± 0.4%, 87 ± 3%, and 40 ± 0.0% adsorption for 10 μM PFOA, PFOS, and GenX, respectively (Fig. 3a).

GenX exhibited the lowest defluorination (33% ± 7%) compared to PFOA (69% ± 10%) and PFOS (51% ± 2%) over 7 h of photocatalysis (Fig. 3b). The total fluorine mole balance for GenX reached a plateau at approximately 100% after 2 h (Fig. 3b), indicating that nearly all organic (67%) and inorganic (33%) fluorine was present in the water phase, with no further transformation observed between 2 and 7 h.

For PFOA, the total fluorine mole balance reached 100% after 7 h, showing that PFOA-bound fluorine was transformed to 1% and 37% organic fluorine in C5-7 and C2-4 PFCAs, respectively, and 69% inorganic fluorine (Fig. 3c). The distribution of fluorine in C5-7 PFCAs increased to 20% after 0.5 h and subsequently decreased to 1% after 7 h, while C2-4 PFCAs gradually increased to 37% after 7 h.

Unlike PFOA and GenX, the total fluorine mole balance of PFOS in the water phase steadily increased and reached only 68% after 7 h (Fig. 3d). Similar to PFOA, the amount of fluorine in C5-7 PFCAs increased to 4% after 1 h and then decreased to 2% after 7 h, while C2-4 PFCAs gradually increased to 15% after 7 h.

4. Discussion

4.1. Degradation pathways

Based on the presented results, the proposed degradation pathways for PFOA and PFOS on Fe-zeolite (Fig. 4) are confirmed (Qian et al., 2020, 2021). The parent compound undergoes stepwise shortening by 1 carbon-fluorine bond (-CF_2). Initially, the adsorbed PFOA or PFOS on the Fe-zeolite's surface or pores complex with isolated Fe^{3+} in tetrahedral and octahedral coordination, forming a $[PFAS\text{-}Fe]^{2+}$ complex (Fig. 4 (1)). Subsequently, the cleavage of the $[PFOA\text{-}Fe]^{2+}$ or $[PFOS\text{-}Fe]^{2+}$ complex leads to into $C_7F_{15}COO\bullet$, $C_8F_{17}SO_3\bullet$, and Fe^{2+} (Fig. 4 (2)) through a ligand-to-metal charge transfer process (Qian et al., 2020, 2021). The loss of 1 electron results in stretching the C–C bond connecting the carboxylic group and the perfluorinated alkyl group or C–S bond, leading to decarboxylation and desulfurization reactions resulting in $C_7F_{15}\bullet$ and $C_8F_{17}\bullet$ radicals (Fig. 4 (3)). The process of decarboxylation and desulfurization results in the removal of 2 F^- ions from the α-carbon, resulting in defluorination and chain-shortening (Fig. 4 (3)) (Liu et al., 2021b). The perfluorinated alkyl radicals are unstable and undergo a series of radical reactions and hydrolysis steps (Qian et al., 2020, 2021). The reduced -CF_2 unit during the degradation process transforms into formic acid ($HCOO^-$) and F^- or further into carbon dioxide (CO_2) (Wang et al., 2008). These reactions are the same for both PFOA and PFOS, regardless of the original headgroup of the parent compounds. In this study, all these degradation products were detected, but the results clearly indicate that degradation of the ultra-short-chain C2-4 PFCAs occurs at substantially slower rates than for PFCAs with longer chains.

Compared to PFOA and PFOS, GenX produced 2 mol of ultra-short-chain PFCAs (C2 and C3) per mole of parent compounds degraded (Fig. 2a). Limited literature has proposed a similar degradation pathway for GenX by photocatalysis (Bao et al., 2018; Olvera-Vargas et al., 2022). Hugo Olvera-Vargas et al. (2022) suggested the cleavage of the carboxylic bond of GenX as the initial step in the electro-Fenton reaction using a graphene-Ni foam cathode paired with a boron-doped diamond anode. This results in $C_3F_7-O-C(OH)F(CF_3)$ as the transformation product. Bao et al. (2018) calculated the dissociation energy of bonds for GenX and reported that the cleavage of the ether bond connecting the $CF_3CF_2CF_2\cdot$ and $\cdot OCFCF3COO^-$ fragments required the lowest energy (212.8 kJ/mol). They proposed a pathway starting with the cleavage of the ether bond and noted that the steric hindrance of the -CF_3 group at the α-position could interfere with the reaction.

As the degradation of PFOA and PFOS is initiated by the formation of the $[PFAS\text{-}Fe]^{2+}$ complex, it is plausible that an analogous formation would occur for the GenX molecule. We propose that GenX ($C_3F_7-O-CF(CF_3)-COO^-$) is first adsorbed by Fe^{3+} to form the $[C_3F_7-O-CF(CF_3)COO-Fe]^{2+}$ complex (Equation (3)) by electrostatic interaction and subsequently dissociate into $C_3F_7-O-CF(CF_3)COO\cdot$ and Fe^{2+} (Equation (4)).

$$C_3F_7-O-CF(CF_3)-COO^- + Fe^{3+} \rightarrow [C_3F_7-O-CF(CF_3)COO-Fe]^{2+} \quad (3)$$

$$[C_3F_7-O-CF(CF_3)COO-Fe]^{2+} \rightarrow C_3F_7-O-CF(CF_3)COO\cdot + Fe^{2+} \quad (4)$$

The $C_3F_7-O-CF(CF_3)COO^{\bullet}$ is unstable because of the loss of 1 electron. Therefore, the stretch of the bond between the carboxylic group and the rest of the GenX molecule (R- COO ·) will occur, similar as for PFOA and PFOS (Fig. 4 (3)), resulting in $C_3F_7-O-C^{\bullet}F(CF_3)$ and CO_2 (Fig. 4), as suggested in previous studies (Olvera-Vargas et al., 2022). The cleavage of the ether bond connecting the $C_3F_7\cdot$ and $\cdot OCF(CF_3)COO\cdot$ fragments seem unlikely because of the double radical in the

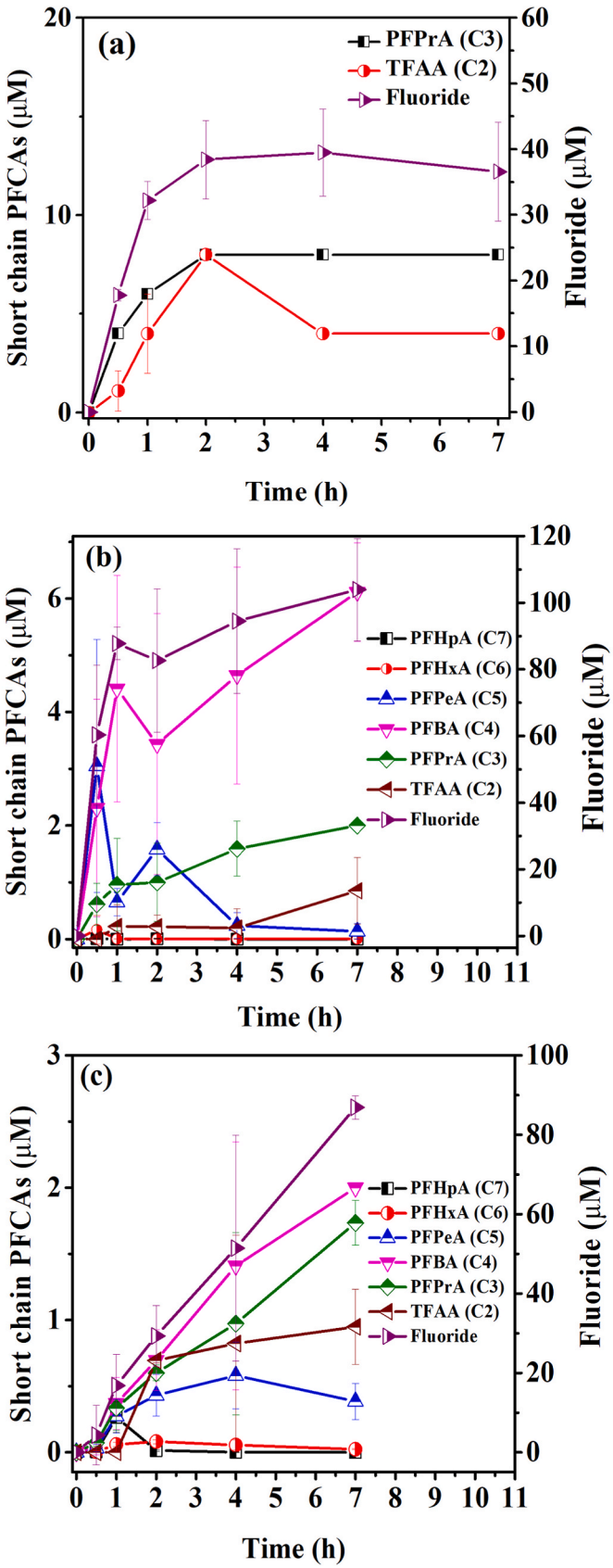

Fig. 2. Concentration of transformation products of GenX (a), PFOA (b) and PFOS (c) produced during the photocatalytic reaction (n = 3).

latter product. Next, the produced $C_3F_7 - O - C^{\bullet}FCF_3$ splits at the ether bond and form $C_3F_7^{\bullet}$ and CF_3CFO. The former radical will be hydrolyzed and defluorinated and then produce PFPrA. The latter radical will hydrolyze and defluorinate to produce TFAA. $HCOO^-$ forms from $-CF_2$ and could be further oxidized into CO_2 and F^- (Wang et al., 2008). We identified 4 transformation products of GenX including formic acid, fluoride, PFPrA and TFAA (**Section 3.2**). However, we could not identify the very first radical intermediates, likely due to their high instability. Following the mechanisms proposed in Fig. 4, PFPrA can be transformed into TFAA by defluorination, and TFAA can be defluorinated and fully demineralized into fluoride, carbon dioxide and H_2O (Olvera-Vargas et al., 2022). However, these reactions didn't take place since the composition in the water phase didn't change anymore after 2 h of reaction (Figs. 1a and 2a).

4.2. Degradation kinetics

A comprehensive analysis of photocatalytic kinetics is challenging due to the intricate involvement of multiple processes, including the sorption-desorption equilibrium between reactants and the catalyst, carrier transfer, transport and recombination of the electrons and holes and the actual photocatalytic reaction (Liu et al., 2014; Deng et al., 2021). The adsorption-desorption equilibrium of PFAS on photocatalysts aligns with the Langmuir-Hinshelwood model (Liu et al., 2014), which successfully fits numerous experimental results of PFAS degradation in photocatalysis (Liu et al., 2014; Sahu et al., 2018; Qian et al., 2020, 2021; Xu et al., 2020). Fig. 3c–d shows that about 73% and 68% of the initial fluorine of PFOA and PFOS transformed into transformation products and fluoride after 30 min and 7 h, respectively. This implies that about 27% and 32%, respectively, of the organic fluorine was either adsorbed on the photocatalyst or potentially transformed by the hydrogen to fluorine (H/F) exchange mechanism into difluoroacetate, monofluoroacetate, or other polyfluorinated intermediates, which were not detected by our LC-MS method (Bentel et al., 2020a). Consequently, utilizing Equation (1) to calculate the apparent rate constant might overestimate the actual degradation rate. To supplement the degradation rate measurements of GenX, PFOA, and PFOS, we calculated the rate of defluorination (Fig. 1c) using a first-order kinetic model.

Comparing degradation rates based on parent PFAS concentration in the water, the order was PFOA > PFOS > GenX. However, considering defluorination, the order changed to PFOA > GenX > PFOS. This demonstrates that relying solely on Equation (1) may not be sufficient to calculate overall PFAS degradation rates on photocatalysts. Some organic fluorine may adsorb on the catalysts and not undergo degradation within the calculated time slot. On the other hand, fluoride is unlikely to adsorb on the photocatalysts, making the rate of defluorination as calculated by Equation (2) a more accurate measure of the overall PFAS degradation rate.

This study used tailor-made flat and wide photocatalysis quartz reactors with 12 cm diameter and 1.8 cm height (with quartz lids). As the UV lights were positioned above the reactors, our designs offer increased exposure to UV light compared to tall and narrow reactors. Stirrers are omitted in the photocatalysis setup to prevent splashing. Due to the lack of stirring, adsorption kinetics may be limited and the obtained reaction rates may be an underestimation (Duan et al., 2022).

The photocatalytic defluorination of PFAS by zeolite and Fe-zeolite is scarcely studied, even though its semiconductor nature has been applied for the photodegradation of dyes (Rubab et al., 2021; Mohamed et al., 2022). Previous studies using Fe-zeolite (Qian et al., 2020, 2021) achieved 38 ± 1% PFOA defluorination (365 nm) in 24 h and 56% PFOS defluorination (254 nm) in 96 h at pH 5.5 with 1 g/L Fe-zeolite. Using rather similar conditions with an Fe-zeolite concentration of 1 g/L and initial pH of 4.4 ± 0.74, we achieved substantially higher defluorination of 69% for PFOA and 51% for PFOS in 7 h. Furthermore, Qian et al. (2020) reported no degradation of PFOA by unmodified zeolite after 24

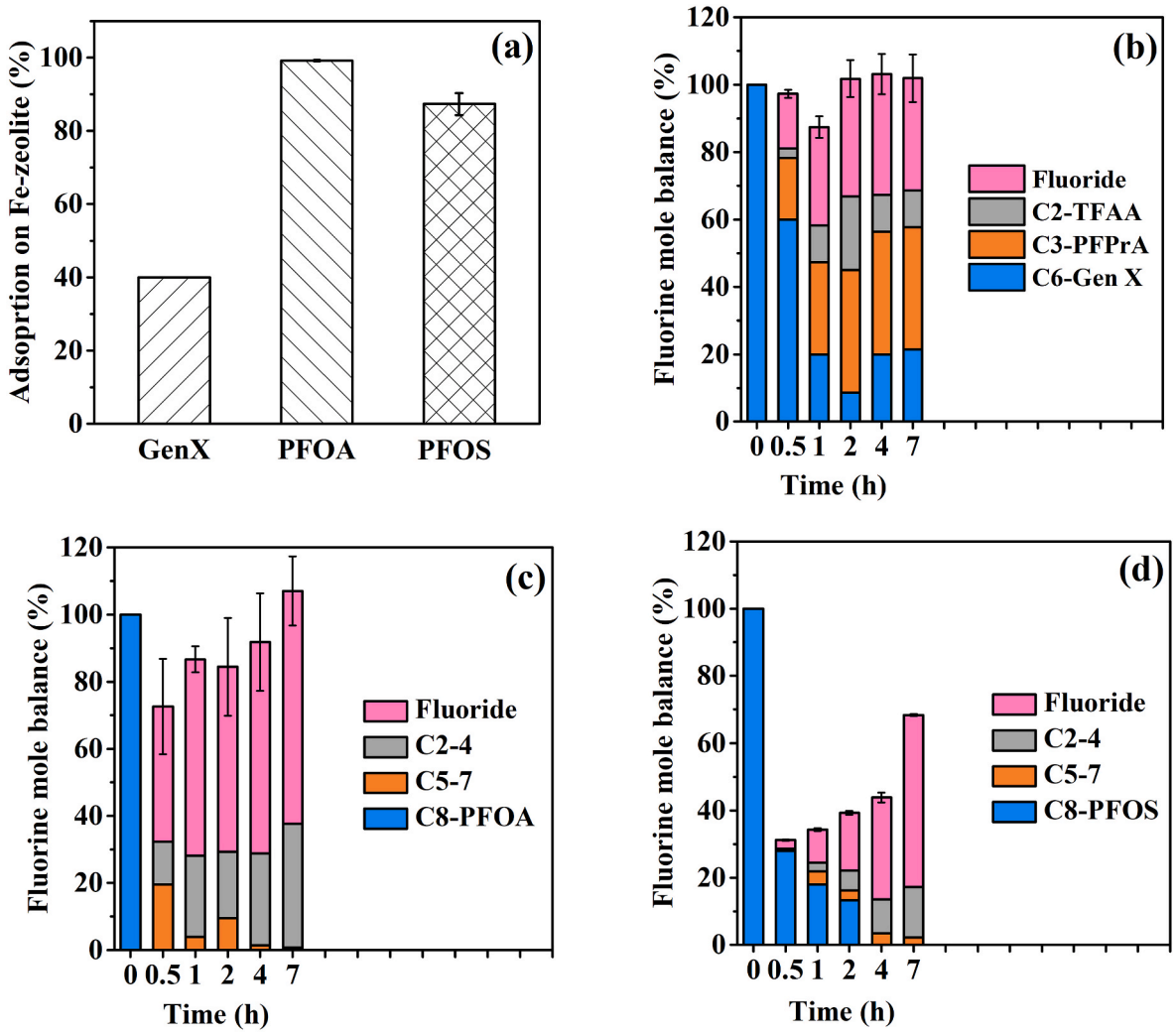

Fig. 3. Adsorption of PFAS (10 μM) onto the Fe-zeolite (1 g/L) overnight (a). Fluorine mole balance of GenX (b), PFOA (c) and PFOS (d) during the photocatalytic reaction. The error bars show the standard deviation of the total mole balance (n = 3).

h of 365 nm UV irradiation at 365 nm. However, we showed that UV radiation of 254 nm with a high energy can effectively defluorinated PFOA (39 ±8% in 7 h). Nevertheless, Fe-zeolite showed superior defluorination. To the best of our knowledge, it is the first time that unmodified zeolite β, hydrogen showed photocatalytic defluorination of PFOA, PFOS and GenX under UV irradiation (Fig. S1). For PFOA, the most studied PFAS, defluorination efficiencies compiled in a recent review ranged from 20% in 12 h using a TiO_2-graphene oxide composite to 90.9% in 4 h using silica-based granular media containing TiO_2 (Zango et al., 2023). Although our 69% defluorination in 7 h is in the higher range, illustrating the high potential of Fe-zeolite, more systematic studies are needed for sound comparisons of the defluorination efficacy across photocatalysts.

4.3. Poor adsorption limits defluorination of ultra-short chain PFCAs

Adsorption of PFAS on inorganic materials such as Fe-zeolite has been explained by a combination of hydrophobic and electrostatic interactions, and steric effects (Ochoa-Herrera and Sierra-Alvarez, 2008; Bao et al., 2018; Li et al., 2023). As a measure of hydrophobicity, the estimated octanol/water partition coefficient of GenX (log K_{ow} of 4.0) (Hopkins et al., 2018) is lower than for PFOA (4.59) (Martz et al., 2019) and PFOS (4.49) (Gu et al., 2023). Hence, the lower hydrophobicity of GenX as compared to PFOA and PFOS would result in weaker hydrophobic interactions which can be associated to the lower adsorption of GenX (40%) on the photocatalyst as compared to PFOA (99%) and PFOS (87%) (Fig. 3a). Even though the electrostatic interactions between Fe^{3+} and the carboxylate group could facilitate the binding of GenX, the steric hindrance from $–CF_3$ bond on GenX could interfere with the oxidation reaction of GenX with Fe^{3+}. The combination of lower adsorption and steric hindrance can explain the lower rate at which GenX was removed from the water phase (Fig. 1b). In addition, branched perfluoroalkyl ether carboxylic acids, such as GenX, have been shown to exhibit lower defluorination compared to linear PFAS due to more prevalent hydrogen to fluorine (H/F) exchange of the branching $–CF_3$ at α-position and forms $C_2F_5CF_2OCH_2COOH$ intermediates (Bentel et al., 2020b). These intermediates are persistent to further degradation (Bentel et al., 2020b), but were not detected by our LC-MS analysis. Furthermore, GenX defluorination reached a plateau already after 2 h, after which no further change in the composition of the degradation products took place (Fig. 3b). That is substantially faster than for PFOA and PFOS. The defluorination of PFOA reached a plateau after 4–7 h and PFOS defluorination was still ongoing after 7 h (Fig. 3c–d). This illustrates that in heterogenous catalysis, considering only the removal rate of parent compounds from the water phase is an incomplete description of the process. To understand the overall rate of defluorination, future work should consider the concentration of parent compound and transformation products in both the water phase and on the catalyst in

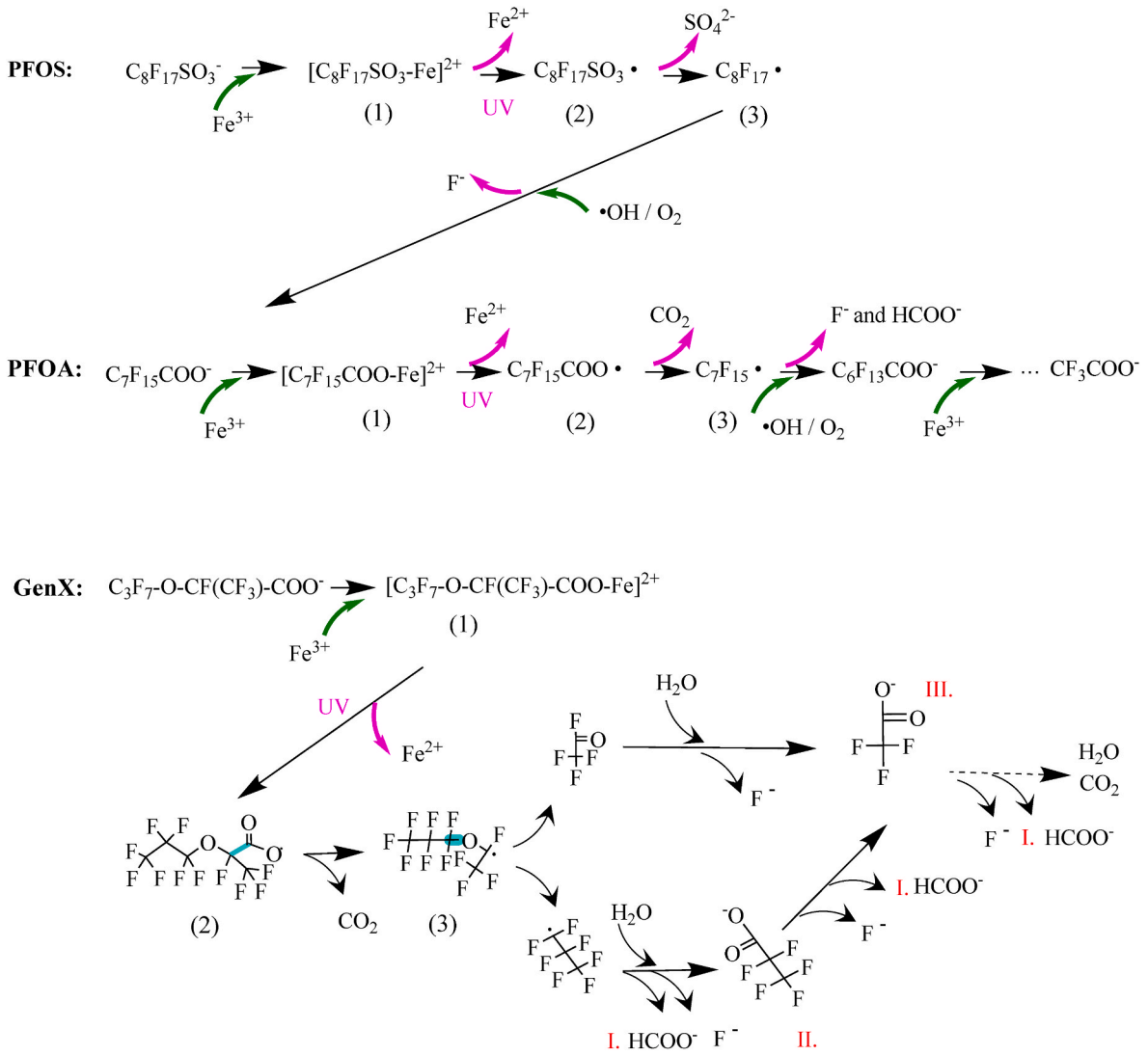

Fig. 4. The degradation pathway of PFOA, PFOS and GenX.

order to provide a more detailed description of the rate of adsorption and the rate of degradation of parent compound and transformation products.

We proposed a degradation pathway for GenX, leading to the formation of PFPrA (C3) and TFAA (C2) as identified transformation products. Stoichiometrically, GenX degradation resulted in 2 mol of ultra-short-chain PFCAs per mole of GenX degraded. In contrast, PFOA and PFOS degraded through stepwise defluorination, producing 1 mol of PFCA products with a gradually shortening chain length (from 7 to 2 carbon atoms) and only 1 mol of terminal degradation products per mole of parent compound. The presence of C2-4 PFCA transformation products have been observed in previous studies with PFOA and PFOS using Fe-zeolite (Qian et al., 2020, 2021).

The ultra-short-chain PFCA transformation products of GenX showed resistance to photocatalysis, likely due to their low hydrophobicity and poor adsorption on the photocatalyst. TFAA has a low hydrophobicity with log K_{ow} of 0.5 (EPA, 2004), while PFPrA (C3) is estimated to have a log K_{ow} between TFAA (C2) and PFBA (C4), which has a log K_{ow} of 1.88 (Zhao et al., 2016). The poor adsorption of short-chain PFAS has been related to their low hydrophobicity in literature reporting that both TFAA and PFPrA exhibit minimal adsorption (less than 10%) onto the Fe-zeolite at a pH of 5.5, as opposed to the observed increasing adsorption of 10–90% for perfluoroalkyl carboxylic acids featuring increasing chain length of 4–8 carbons (Qian et al., 2020). The combination of producing a higher number of ultra-short-chain PFCA transformation products with poor adsorption explains the overall lower defluorination of GenX compared to PFOA and PFOS (Fig. 3b).

5. Conclusion

GenX exhibited the lowest removal (79%) and defluorination (33%) after 7 h of photocatalysis, compared to PFOA (100% removal and 69% defluorination) and PFOS (100% removal and 51% defluorination). The quasi-first-order degradation rate of GenX (1.5 h^{-1}) was 12 times lower than PFOA (18.4 h^{-1}) and 1.2 times lower than PFOS (1.8 h^{-1}). The fluoride formation rate for PFOA (0.9 h^{-1}) was approximately 2.6 times higher than GenX (0.35 h^{-1}) and 9 times higher than PFOS (0.1 h^{-1}).

Linear PFAS like PFOA and PFOS undergo stepwise defluorination, producing gradually shortening PFCAs as transformation products. In contrast, branched PFAS like GenX produce 2 mol of ultra-short PFCAs (TFAA (C2) and PFPrA (C3)) per mole of GenX degraded. However, all tested PFAS, including the ultra-short-chain PFCA transformation products (TFAA (C2), PFPrA (C3), and PFBA (C4)), exhibited slow degradation, likely due to poor adsorption to the photocatalyst, leading to their accumulation in the water phase over time.

The total fluorine mole balance showed that GenX degradation reached a plateau after 2 h, while PFOA degradation reached a plateau after 4–7 h, and PFOS degradation was still ongoing after 7 h. The poorer

degradation and defluorination of GenX compared to PFOA and PFOS could be attributed to its lower adsorption on the catalyst, possible steric hindrance of $–CF_3$ at the α position and H/F exchange, and the production of more ultra-short chain transformation products that are not further degraded due to poor adsorption on the catalyst.

CRediT authorship contribution statement

Junying Wen: Methodology, Formal analysis, Investigation, Writing – original draft, Visualization. **Huarui Li:** Investigation. **Lars Ottosen:** Funding acquisition. **Johan Lundqvist:** Supervision, Writing – review & editing. **Leendert Vergeynst:** Conceptualization, Methodology, Writing – review & editing, Supervision, Funding acquisition, Project administration.

Declaration of competing interest

The authors declare that they have no known competing financial interests or personal relationships that could have appeared to influence the work reported in this paper.

Data availability

Data will be made available on request.

Acknowledgements

Thomas Dyekjær from the Department of Biological and Chemical Engineering, Aarhus University, is gratefully acknowledged for excellently supporting the LC-MS operation. This work was supported by a research grant from the Aarhus University Centre for Water Technology (WATEC), the Poul Due Jensen Foundation, Denmark, and a PhD scholarship from the Aarhus University Graduate School of Technical Sciences.

Appendix A. Supplementary data

Supplementary data to this article can be found online at https://doi.org/10.1016/j.chemosphere.2023.140344.

References

Arana Juve, J.-M., Li, F., Zhu, Y., Liu, W., Ottosen, L.D.M., Zhao, D., Wei, Z., 2022. Concentrate and degrade PFOA with a photo-regenerable composite of In-doped TNTs@AC. Chemosphere 300, 134495. https://doi.org/10.1016/j.chemosphere.2022.134495.

Ašperger, S., 2003. Chemical kinetics and reaction mechanisms. In: Ašperger, S. (Ed.), Chemical Kinetics and Inorganic Reaction Mechanisms. Springer US, Boston, MA, pp. 3–103.

Bao, Y., Deng, S., Jiang, X., Qu, Y., He, Y., Liu, L., Chai, Q., Mumtaz, M., Huang, J., Cagnetta, G., Yu, G., 2018. Degradation of PFOA substitute: GenX (HFPO–DA ammonium salt): oxidation with UV/persulfate or reduction with UV/sulfite? Environ. Sci. Technol. 52, 11728–11734. https://doi.org/10.1021/acs.est.8b02172.

Bentel, M.J., Liu, Z., Yu, Y., Gao, J., Men, Y., Liu, J., 2020a. Enhanced degradation of perfluorocarboxylic acids (PFCAs) by UV/sulfite treatment: reaction mechanisms and system efficiencies at pH 12. Environ. Sci. Technol. Lett. 7, 351–357. https://doi.org/10.1021/acs.estlett.0c00236.

Bentel, M.J., Yu, Y., Xu, L., Kwon, H., Li, Z., Wong, B.M., Men, Y., Liu, J., 2020b. Degradation of perfluoroalkyl ether carboxylic acids with hydrated electrons: structure–reactivity relationships and environmental implications. Environ. Sci. Technol. 54, 2489–2499. https://doi.org/10.1021/acs.est.9b05869.

Crone, B.C., Speth, T.F., Wahman, D.G., Smith, S.J., Abulikemu, G., Kleiner, E.J., Pressman, J.G., 2019. Occurrence of per- and polyfluoroalkyl substances (PFAS) in source water and their treatment in drinking water. Crit. Rev. Environ. Sci. Technol. 49, 2359–2396. https://doi.org/10.1080/10643389.2019.1614848.

Deng, Y., Liang, Z., Lu, X., Chen, D., Li, Z., Wang, F., 2021. The degradation mechanisms of perfluorooctanoic acid (PFOA) and perfluorooctane sulfonic acid (PFOS) by different chemical methods: a critical review. Chemosphere 283, 131168. https://doi.org/10.1016/j.chemosphere.2021.131168.

Duan, L., Wang, B., Heck, K.N., Clark, C.A., Wei, J., Wang, M., Metz, J., Wu, G., Tsai, A.-L., Guo, S., Arredondo, J., Mohite, A.D., Senftle, T.P., Westerhoff, P., Alvarez, P., Wen, X., Song, Y., Wong, M.S., 2022. Titanium oxide improves boron nitride photocatalytic degradation of perfluorooctanoic acid. Chem. Eng. J. 448, 137735. https://doi.org/10.1016/j.cej.2022.137735.

ECHA, 2019. Candidate List of substances of very high concern for Authorisation. https://www.echa.europa.eu/candidate-list-table.

EPA, 2019. United States environmental protection. In: Method 533: determination Of Per- And Polyfluoroalkyl Substances In Drinking Water By Isotope Dilution Anion Exchange Solid Phase Extraction And Liquid Chromatography/Tandem Mass Spectrometry. EPA United States Environmental Protection, the United States.

EPA, 2022. Final Health Advisories for GenX Chemicals and PFBS. The United States Envionmental Protection Agency, The United States. https://www.epa.gov/sdwa/drinking-water-health-advisories-genx-chemicals-and-pfbs.

EPA, U., 2004. Estimation Program Interface (EPI) Suite.

Evans, N., Conley, J.M., Cardon, M., Hartig, P., Medlock-Kakaley, E., Gray, L.E., 2022. In vitro activity of a panel of per- and polyfluoroalkyl substances (PFAS), fatty acids, and pharmaceuticals in peroxisome proliferator-activated receptor (PPAR) alpha, PPAR gamma, and estrogen receptor assays. Toxicol. Appl. Pharmacol. 449, 116136 https://doi.org/10.1016/j.taap.2022.116136.

Gebbink, W.A., van Asseldonk, L., van Leeuwen, S.P.J., 2017. Presence of emerging per- and polyfluoroalkyl substances (PFASs) in river and drinking water near a fluorochemical production plant in The Netherlands. Environ. Sci. Technol. 51, 11057–11065. https://doi.org/10.1021/acs.est.7b02488.

Glüge, J., Scheringer, M., Cousins, I.T., Dewitt, J.C., Goldenman, G., Herzke, D., Lohmann, R., Ng, C.A., Trier, X., Wang, Z., 2020. An overview of the uses of per- and polyfluoroalkyl substances (PFAS). Environ. Sci.: Process. Impacts 22, 2345–2373. https://doi.org/10.1039/d0em00291g.

Gu, Q., Wen, Y., Wu, H., Cui, X., 2023. Uptake and translocation of both legacy and emerging per- and polyfluorinated alkyl substances in hydroponic vegetables. Sci. Total Environ. 862, 160684 https://doi.org/10.1016/j.scitotenv.2022.160684.

Hopkins, Z.R., Sun, M., DeWitt, J.C., Knappe, D.R.U., 2018. Recently detected drinking water contaminants: GenX and other per- and polyfluoroalkyl ether acids. J. AWWA (Am. Water Works Assoc.) 110, 13–28. https://doi.org/10.1002/awwa.1073.

Jamalluddin, N.A., Abdullah, A.Z., 2014. Low frequency sonocatalytic degradation of Azo dye in water using Fe-doped zeolite y catalyst. Ultrason. Sonochem. 21, 743–753. https://doi.org/10.1016/j.ultsonch.2013.10.008.

Janda, J., Nödler, K., Brauch, H.-J., Zwiener, C., Lange, F.T., 2019. Robust trace analysis of polar (C2-C8) perfluorinated carboxylic acids by liquid chromatography-tandem mass spectrometry: method development and application to surface water, groundwater and drinking water. Environ. Sci. Pollut. Control Ser. 26, 7326–7336. https://doi.org/10.1007/s11356-018-1731-x.

Li, H., Junker, A.L., Wen, J., Ahrens, L., Sillanpää, M., Tian, J., Cui, F., Vergeynst, L., Wei, Z., 2023. A recent overview of per- and polyfluoroalkyl substances (PFAS) removal by functional framework materials. Chem. Eng. J. 452, 139202 https://doi.org/10.1016/j.cej.2022.139202.

Li, Y., Fletcher, T., Mucs, D., Scott, K., Lindh, C.H., Tallving, P., Jakobsson, K., 2018a. Half-lives of PFOS, PFHxS and PFOA after end of exposure to contaminated drinking water. Occup. Environ. Med. 75, 46–51. https://doi.org/10.1136/oemed-2017-104651.

Li, Y., Fletcher, T., Mucs, D., Scott, K., Lindh, C.H., Tallving, P., Jakobsson, K., 2018b. Half-lives of PFOS, PFHxS and PFOA after end of exposure to contaminated drinking water. Occup. Environ. Med. 75, 46. https://doi.org/10.1136/oemed-2017-104651.

Liu, B., Zhao, X., Terashima, C., Fujishima, A., Nakata, K., 2014. Thermodynamic and kinetic analysis of heterogeneous photocatalysis for semiconductor systems. Phys. Chem. Chem. Phys. 16, 8751–8760. https://doi.org/10.1039/C3CP55317E.

Liu, L., Qu, Y., Huang, J., Weber, R., 2021a. Per- and polyfluoroalkyl substances (PFASs) in Chinese drinking water: risk assessment and geographical distribution. Environ. Sci. Eur. 33, 6. https://doi.org/10.1186/s12302-020-00425-3.

Liu, Z., Bentel, M.J., Yu, Y., Ren, C., Gao, J., Pulikkal, V.F., Sun, M., Men, Y., Liu, J., 2021b. Near-quantitative defluorination of perfluorinated and fluorotelomer carboxylates and sulfonates with integrated oxidation and reduction. Environ. Sci. Technol. 55, 7052–7062. https://doi.org/10.1021/acs.est.1c00353.

Liu, Z., Chen, Z., Gao, J., Yu, Y., Men, Y., Gu, C., Liu, J., 2022. Accelerated degradation of perfluorosulfonates and perfluorocarboxylates by UV/sulfite + iodide: reaction mechanisms and system efficiencies. Environ. Sci. Technol. 56, 3699–3709. https://doi.org/10.1021/acs.est.1c07608.

Martz, M., Heil, J., Marschner, B., Stumpe, B., 2019. Effects of soil organic carbon (SOC) content and accessibility in subsoils on the sorption processes of the model pollutants nonylphenol (4-n-NP) and perfluorooctanoic acid (PFOA). Sci. Total Environ. 672, 162–173. https://doi.org/10.1016/j.scitotenv.2019.03.369.

Mohamed, F., Hassaballa, S., Shaban, M., Ahmed, A.M., 2022. Highly Efficient Photocatalyst Fabricated from the Chemical Recycling of Iron Waste and Natural Zeolite for Super Dye Degradation. Nanomaterials 12, p. 235.

Ochoa-Herrera, V., Sierra-Alvarez, R., 2008. Removal of perfluorinated surfactants by sorption onto granular activated carbon, zeolite and sludge. Chemosphere 72, 1588–1593. https://doi.org/10.1016/j.chemosphere.2008.04.029.

Olvera-Vargas, H., Wang, Z., Xu, J., Lefebvre, O., 2022. Synergistic degradation of GenX (hexafluoropropylene oxide dimer acid) by pairing graphene-coated Ni-foam and boron doped diamond electrodes. Chem. Eng. J. 430, 132686 https://doi.org/10.1016/j.cej.2021.132686.

Pierozan, P., Karlsson, O., 2021. Differential susceptibility of rat primary neurons and neural stem cells to PFOS and PFOA toxicity. Toxicol. Lett. 349, 61–68. https://doi.org/10.1016/j.toxlet.2021.06.004.

Qian, L., Georgi, A., Gonzalez-Olmos, R., Kopinke, F.-D., 2020. Degradation of perfluorooctanoic acid adsorbed on Fe-zeolites with molecular oxygen as oxidant under UV-A irradiation. Appl. Catal. B Environ. 278, 119283 https://doi.org/10.1016/j.apcatb.2020.119283.

Qian, L., Kopinke, F.-D., Georgi, A., 2021. Photodegradation of perfluorooctanesulfonic acid on Fe-zeolites in water. Environ. Sci. Technol. 55, 614–622. https://doi.org/10.1021/acs.est.0c04558.

Rahman, M.F., Peldszus, S., Anderson, W.B., 2014. Behaviour and fate of perfluoroalkyl and polyfluoroalkyl substances (PFASs) in drinking water treatment: a review. Water Res. 50, 318–340.

Rubab, M., Bhatti, I.A., Nadeem, N., Shah, S.A.R., Yaseen, M., Naz, M.Y., Zahid, M., 2021. Synthesis and photocatalytic degradation of rhodamine B using ternary zeolite/WO(3)/Fe(3)O(4)composite. Nanotechnology 32. https://doi.org/10.1088/1361-6528/ac037f.

Sahu, S.P., Qanbarzadeh, M., Ateia, M., Torkzadeh, H., Maroli, A.S., Cates, E.L., 2018. Rapid degradation and mineralization of perfluorooctanoic acid by a new petitjeanite Bi3O(OH)(PO4)2 microparticle ultraviolet photocatalyst. Environ. Sci. Technol. Lett. 5, 533–538. https://doi.org/10.1021/acs.estlett.8b00395.

Thompson, J., Eaglesham, G., Mueller, J., 2011. Concentrations of PFOS, PFOA and other perfluorinated alkyl acids in Australian drinking water. Chemosphere 83, 1320–1325. https://doi.org/10.1016/j.chemosphere.2011.04.017.

Vakili, M., Bao, Y., Gholami, F., Gholami, Z., Deng, S., Wang, W., Kumar Awasthi, A., Rafatullah, M., Cagnetta, G., Yu, G., 2021. Removal of HFPO-DA (GenX) from aqueous solutions: a mini-review. Chem. Eng. J. 424, 130266 https://doi.org/10.1016/j.cej.2021.130266.

Vergeynst, L., K'Oreje, K., De Wispelaere, P., Harinck, L., Van Langenhove, H., Demeestere, K., 2017. Statistical procedures for the determination of linearity, detection limits and measurement uncertainty: a deeper look into SPE-LC-Orbitrap mass spectrometry of pharmaceuticals in wastewater. J. Hazard Mater. 323, 2–10. https://doi.org/10.1016/j.jhazmat.2016.05.077.

Wang, Y., Zhang, P., Pan, G., Chen, H., 2008. Ferric ion mediated photochemical decomposition of perfluorooctanoic acid (PFOA) by 254nm UV light. J. Hazard Mater. 160, 181–186. https://doi.org/10.1016/j.jhazmat.2008.02.105.

Wen, Y., Rentería-Gómez, Á., Day, G.S., Smith, M.F., Yan, T.-H., Ozdemir, R.O.K., Gutierrez, O., Sharma, V.K., Ma, X., Zhou, H.-C., 2022. Integrated photocatalytic reduction and oxidation of perfluorooctanoic acid by metal–organic frameworks: key insights into the degradation mechanisms. J. Am. Chem. Soc. 144, 11840–11850. https://doi.org/10.1021/jacs.2c04341.

Xia, C., Lim, X., Yang, H., Goodson, B.M., Liu, J., 2022. Degradation of per- and polyfluoroalkyl substances (PFAS) in wastewater effluents by photocatalysis for water reuse. J. Water Proc. Eng. 46, 102556 https://doi.org/10.1016/j.jwpe.2021.102556.

Xu, T., Zhu, Y., Duan, J., Xia, Y., Tong, T., Zhang, L., Zhao, D., 2020. Enhanced photocatalytic degradation of perfluorooctanoic acid using carbon-modified bismuth phosphate composite: effectiveness, material synergy and roles of carbon. Chem. Eng. J. 395, 124991 https://doi.org/10.1016/j.cej.2020.124991.

Yoo, H.J., Pyo, M.C., Park, Y., Kim, B.Y., Lee, K.W., 2021. Hexafluoropropylene oxide dimer acid (GenX) exposure induces apoptosis in HepG2 cells. Heliyon 7, e08272. https://doi.org/10.1016/j.heliyon.2021.e08272.

Zango, Z.U., Khoo, K.S., Garba, A., Kadir, H.A., Usman, F., Zango, M.U., Da Oh, W., Lim, J.W., 2023. A review on superior advanced oxidation and photocatalytic degradation techniques for perfluorooctanoic acid (PFOA) elimination from wastewater. Environ. Res. 221, 115326 https://doi.org/10.1016/j.envres.2023.115326.

Zhao, P., Xia, X., Dong, J., Xia, N., Jiang, X., Li, Y., Zhu, Y., 2016. Short- and long-chain perfluoroalkyl substances in the water, suspended particulate matter, and surface sediment of a turbid river. Sci. Total Environ. 568, 57–65. https://doi.org/10.1016/j.scitotenv.2016.05.221.

Zhu, Y., Ji, H., He, K., Blaney, L., Xu, T., Zhao, D., 2022. Photocatalytic degradation of GenX in water using a new adsorptive photocatalyst. Water Res. 220, 118650 https://doi.org/10.1016/j.watres.2022.118650.